Explaining the Absence of Co-58 Radiation Fields Around CANDU Reactor Primary Circuit

K.A. BURRILL AND D.A. GUZONAS
AECL
CHALK RIVER LABORATORIES
CHALK RIVER, ON

Abstract

Radiation fields from Co-58 are rarely detected in CANDU plants. For example, Ge(Li) surveys of the Inconel 600 steam generators at some CANDU plants may show radiation attributed to Co-58 only early in plant life, and most artefacts removed from the primary circuit later in plant operation show no Co-58 present. However, Pressurized Water Reactor plants experience relatively large fields from Co-58 on their isothermal piping, e.g., steam generator channel head, and steam generators tube sampling programs do show deposits in the tubes with significant Co-58 compared to other radionuclides such as Co-60.

CANDU reactors have high concentrations of dissolved iron due to the extensive use of carbon steel for the isothermal piping, e.g., feeders, headers, and steam generator channel heads. A dissolved iron transport diagram that was proposed recently for the primary circuit of CANDU plants has been validated by comparison of predicted deposit weights with plant deposit data from various components. One feature of the diagram is dissolved iron precipitation inside the steam generators tubes. An hypothesis is advanced here in which precipitating dissolved iron is proposed to occlude dissolved nickel. This removal mechanism may prevent the solubility of dissolved nickel from being exceeded anywhere around the primary circuit. In particular, this mechanism could avoid NiO precipitation in the core and the generation of large quantities of Co-58. Using this mechanism along with the known solubility behaviour of NiO with temperature, a dissolved nickel transport diagram has been proposed for CANDU plants.

A simple model of the hypothesis has been made to describe the dissolved nickel concentration in the coolant in the steam generator tubes. Nickel is being supplied to the boundary layer of water at the tube surface by Inconel 600 corrosion product release as well as by mass transfer from the bulk coolant and the model predicts a slow rise in the Ni/Fe ratio in the magnetite deposits with distance along the steam generator tubes. In this model, it was assumed that both Fe and Ni could substitute equally in one particular lattice site in the depositing species. Support for this model is provided by good agreement with Bruce Power data from four steam generator tubes in Unit 3, which show Ni/Fe = 0.02 in the magnetite deposits. Precipitation of the dissolved iron inside the steam generator tubes therefore may be viewed as a powerful purification process for CANDU plants. This purification mechanism can be extended to cobalt as Secondary Ion Mass Spectrometry data for a magnetite deposit on an Incoloy 800 steam generator tube from a CANDU 6 plant show the Ni and Co concentrations are constant throughout the depth of the 120 μm thick deposit except within 10 μm of the corrosion film on the tube.

Based on the above work, transport diagrams for dissolved Fe and Ni are postulated for Pressurized Water Reactors in which coordinated water chemistry now results in Fe precipitation in the steam generator tubes rather than onto the fuel cladding. However, insufficient Fe precipitation apparently still results in dissolved Ni exceeding its solubility in-core and there is precipitation especially in regions with subcooled nucleate boiling. This may be the origin of the Ni-rich deposits seen in this region and they may provide the porous matrix in which boiling can concentrate dissolved species such as LiOH and boric acid. One consequence is the Axial Offset Anomaly observed in some plants.

1. Introduction

Radiation fields from Co-58 are detected only in the first year of operation in CANDU plants. After extended operation, Ge(Li) surveys of the Inconel 600 steam generators (SG) at the Bruce NGS do not show any radiation attributed to this radionuclide. Examination of reactor artefacts indicate only small amounts of Co-58 are present in the primary side deposits. Measurements of the crud deposits on Pickering and Bruce fuel sheath surfaces does show some Co-58 in the extremely light deposits, and is presumed to be formed from irradiation of NiO particles mixed in with the iron-rich crud particles, chiefly magnetite. However, Co-58 generated from this particle deposition/irradiation/dissolution process, and possibly recoil, is not significant compared to Co-60, Zr-95, Sb-124, and fission products. In contrast, PWR plants have experienced relatively large fields from Co-58 on their isothermal piping, e.g., steam generator channel head (Vernon, 1982; Fero, 1983) and SG tube sampling programs do show deposits in the tubes with significant Co-58, e.g., Bergmann et al. (1983), compared to other radionuclides such as Co-60.

CANDU® is a registered trademark of Atomic Energy of Canada Limited (AECL).

The lack of a Co-58 radiation field around the CANDU Heat Transport System (HTS) has been puzzling, especially when Inconel 600 tubing is used in the steam generators, as at Bruce NGS. Interest in the behaviour of dissolved nickel has now arisen in the EPRI program addressing the Axial Offset Anomaly (AOA) observed in some PWRs, e.g., Callaway. Frattini et al. (2000) have reported that their in-core deposit flake from Callaway was rich in Ni, with some Fe and with layers of ZrO_2 and boron-rich bonnacordite. The coordinated water chemistry used in the heat transport system (HTS) of PWRs now provides a normal solubility curve for magnetite so that any iron released by stainless steel and Inconel 600 (or 690) corrosion will be precipitated on the cold leg of the SG and no longer be precipitated in-core. However, nickel oxide solubility declines with increasing temperature for all pH_T, e.g., pH_T 6.9-7.4 with T in the range 260-320°C and the water contains nominally 35 mL H_2/kg. The solubility is about 0.1 μg Ni/kg at 300°C (Fruzzetti and Sawochka, 2000). Therefore, NiO may be precipitating in-core on the fuel sheathing, especially in regions of sub-cooled nucleate boiling.

An hypothesis is advanced here in which precipitating dissolved iron from the primary CANDU coolant in the steam generators also removes dissolved nickel. This mechanism prevents the solubility of dissolved nickel from being exceeded anywhere around the circuit. In particular, this avoids NiO precipitation in-core and the generation of large quantities of Co-58. The hypothesis has been modeled and tested by comparison of the predicted Ni/Fe ratio in Bruce-A steam generator tube deposits with data from deposit measurements on four tubes. A ratio Ni/Fe = 0.02 is predicted and observed. Predictions are also made for an Incoloy-800 tube, and a detailed SIMS examination through the deposit on a similar tube shows that the magnetite deposit holds up cobalt as well as nickel released by tube corrosion.

2. Transport Diagrams for Dissolved Iron and Nickel

The changes in dissolved iron and nickel oxide solubilities around the HTS due to coolant temperature change combine with corrosion product release of iron and nickel to dictate the possible deposition of these solutes on system components somewhere in the HTS. 'Transport diagrams' are presented here for these solutes to show the interaction between these two processes in both CANDU and PWR plants and to show how these diagrams may be used.

2.1 Transport Diagrams for the CANDU Reactor HTS

The dissolved iron transport diagram in Figure 1 was first constructed for CANDU-6 plants, e.g., Burrill (1998), and this transport model has since been quantified by comparison of predicted deposit weights and their distributions with distance along components with plant deposit data from many sources. The model for dissolved iron transport has now been used to extend the activity transport model based on in-core particle deposition and dissolution (Burrill, 1976) to predict radiation field growth at Pickering NGS.

An analogous transport diagram for dissolved nickel transport has now been constructed for CANDU-6 plants as shown in Figure 2. The water is assumed to be saturated in dissolved Ni at the highest temperature reached in the HTS, i.e., at the core outlet. There is no change in the solubility of nickel oxide (S_{Ni}) or the dissolved nickel concentration (C_{Ni}) through the outlet end-fitting and the outlet feeder. Flow accelerated corrosion of the outlet feeder quickly results in a thin magnetite film of steady state thickness so that any Ni removed by the magnetite will be re-introduced to the coolant upon dissolution. The dissolved Ni concentration will begin to rise in the SG tubes because of Ni release by tube corrosion. The transport diagram shows no change in the concentration in the bulk coolant near the tube inlet until all the heavy water steam has been condensed in the tubes: the

condensing steam dilutes the dissolved nickel. Once the steam is condensed, NiO solubility rises as the temperature falls, and there may be enough release by corrosion to exceed the solubility, equal it, or fall short of the increasing solubility. The diagram arbitrarily shows the last case. Once dissolved iron begins to precipitate near the top of the hot leg of the SG tubes, it is hypothesized that Ni competes with Fe for ferrous sites in the magnetite growing from solution, or substitutes for Fe^{2+} in the $Fe(OH)_2$ film that may initially form on the magnetite. When the coolant enters the inlet feeders, there is no longer a supply of dissolved Ni, and an exponential decline in its concentration is expected as it co-precipitates with the magnetite on the feeder surface. This decline continues through the end-fitting and into the core. Detailed calculations are needed to show where the coolant may become supersaturated in dissolved nickel, e.g., with onset of sub-cooled nucleate boiling and bulk boiling. There may be heavier NiO deposits on fuel cladding in the bulk boiling region, compared to the non-boiling region of the fuel channel.

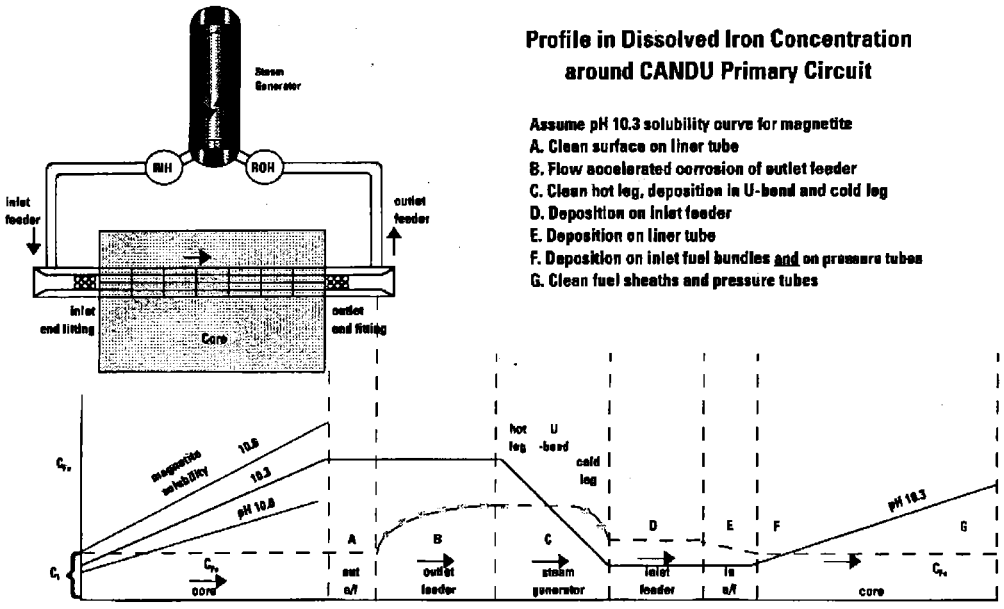

Figure 1. Dissolved Iron Transport Diagram for CANDU 6 Heat Transport System.

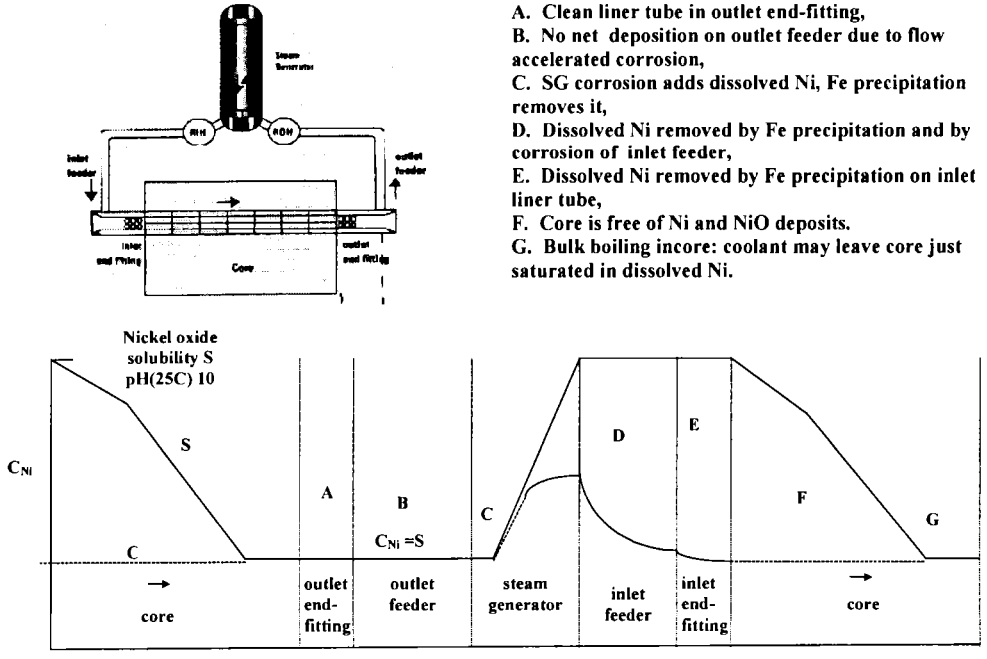

Figure 2. Dissolved Nickel Transport Diagram for CANDU 6 Heat Transport System.

2.2 Transport Diagrams for Pressurized Water Reactors

Figure 3 presents the dissolved iron transport diagram proposed for PWR plants operating with 'coordinated' water chemistry. This chemistry maintains the coolant pH constant at some operating temperature, e.g., pH_{300} 7.0, by adjusting the amount of dissolved LiOH to counter the acidity of the boric acid. The dissolved iron concentration changes little around the HTS compared to the solubility changes for magnetite because of the low corrosion product release rates from stainless steel isothermal piping and from the Inconel 600 or 690 steam generator tubing. Some precipitation of magnetite is postulated at the outlet from the SG tubes and along the core inlet piping.

Figure 4 presents the transport diagram for dissolved nickel. Since there is little removal of Ni by the small amount of magnetite precipitated in the HTS, the dissolved Ni concentration will show relatively wide swings in concentration. In-core, the NiO solubility curve is exceeded and NiO is formed. Any deposition in non-boiling regions of the core will result in conversion of the NiO to metallic nickel due to the highly reducing water chemistry in-core. Sub-cooled and nucleate boiling generates an oxidizing water chemistry around the steam bubbles at the fuel sheathing surface and the deposit will remain as NiO. There should be NiO deposits also formed on the hot-leg isothermal piping if precipitation is mass-transfer controlled in-core. Corrosion product release rates of the SG alloy may be low enough that all released dissolved Ni remains in solution through the SG length. This unsaturation may persist right into the core.

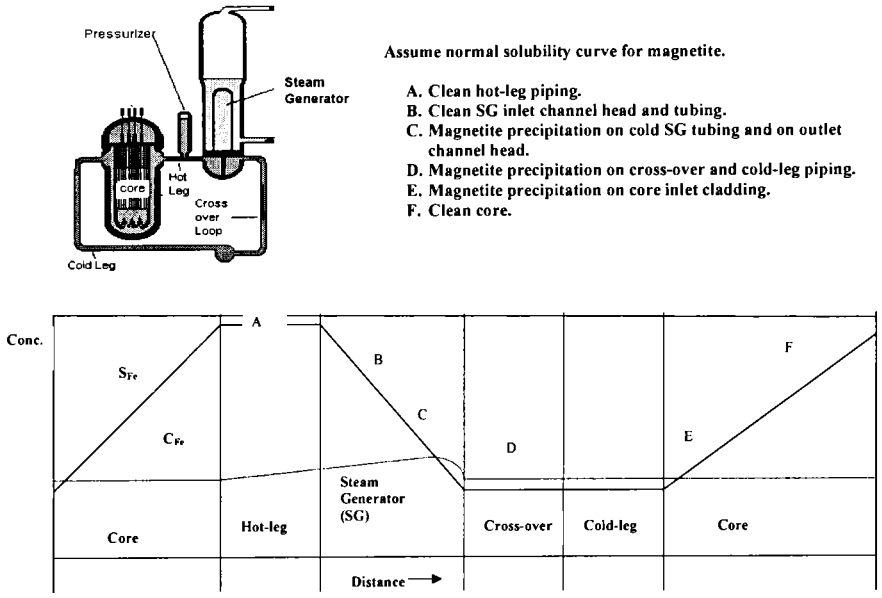

Figure 3. Dissolved Iron Transport Diagram for PWR Primary Circuit.

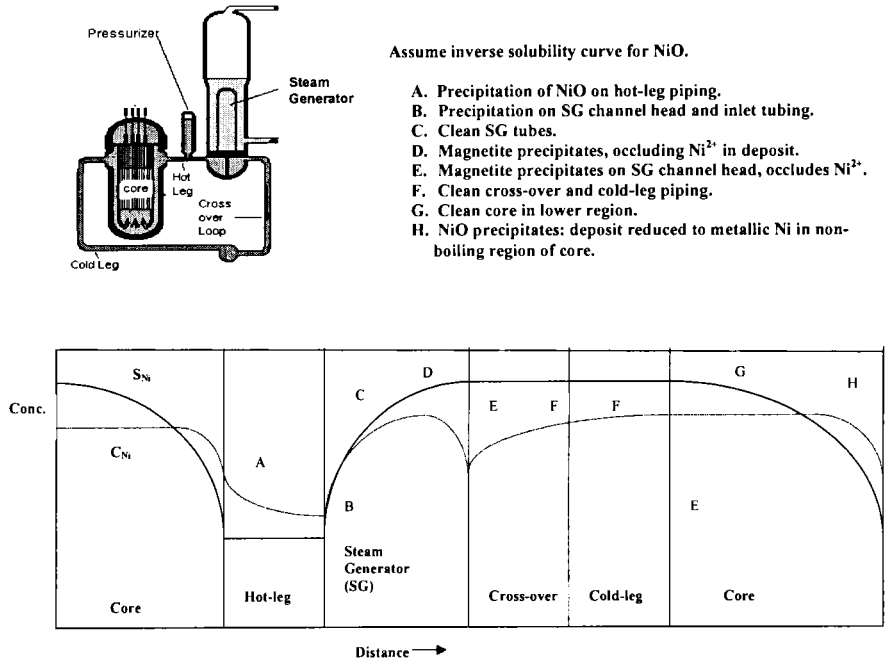

Figure 4. Dissolved Nickel Transport Diagram for PWR Primary Circuit.

These diagrams need to be modeled mathematically with realistic corrosion rates and with a mass-transfer controlled deposition rate for magnetite to determine where magnetite (iron-rich) deposits will be found and their magnitude. Then, calculations with the model presented in this paper are needed to determine the actual behaviour of the dissolved nickel.

3. Nickel Co-Precipitation with Iron in the CANDU Reactor HTS

Details of a model are presented here that predicts the quantity of dissolved nickel co-precipitating with dissolved iron during magnetite precipitation inside CANDU reactor steam generator (SG) tubes.

3.1 Prediction of the Magnetite Deposit Distribution in a SG Tube

Dissolved iron will precipitate as magnetite whenever its solubility is exceeded in water with reducing conditions, e.g., inside SG tubes when the water is cooled. Burrill and Turner (1994) have shown that the predictions of a model for the deposition process compare well with deposit data from the Pickering NGS SG tubes when deposition is controlled by turbulent mass transfer of dissolved iron from the bulk coolant. The Bruce NGS plant uses a feedwater preheater external to the typical CANDU reactor, which has a preheater internal to the SG, and therefore it is a simpler design with which to illustrate the co-precipitation model to be presented here. Figure 5 compares the predictions of the computer code used to evaluate the above iron oxide deposition model with deposit data taken from the U-bend region of a steam generator in Bruce Unit 2 after 9.34 EFPY (Effective Full Power Years). The model predicts that magnetite precipitation begins about 4-6 metres from the SG tube inlet, depending on the dissolved iron concentration in the coolant entering the tubes.

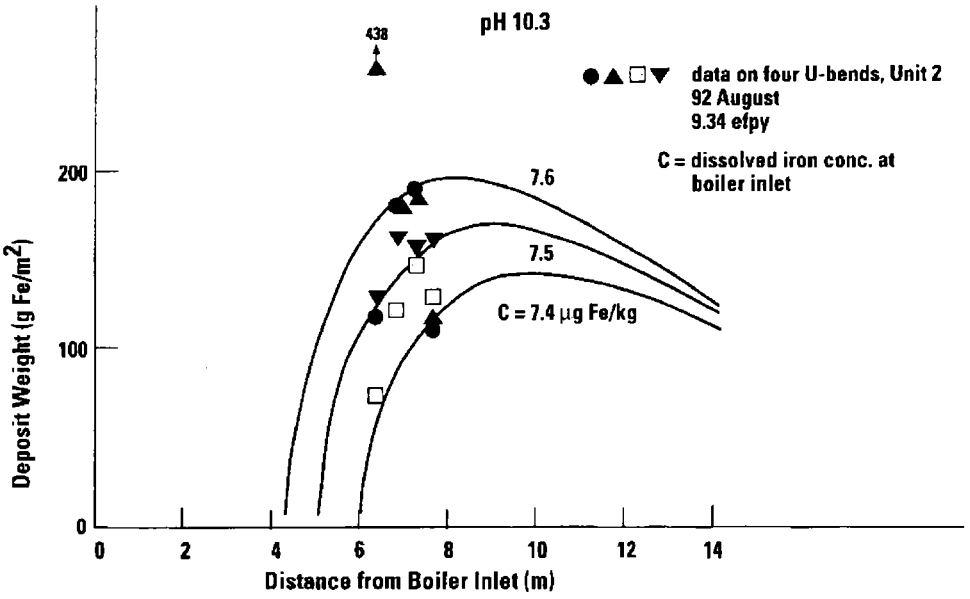

Figure 5. Predicted Deposit Distribution in Bruce-A Boiler from Primary Side Fouling.

3.2 Variations in Coolant Temperatures and Magnetite Solubility in a Bruce SG Tube

The temperature (Tw) of the coolant in the boundary layer of water contacting the wall of a clean SG tube is used to predict the solubility of dissolved iron and dissolved nickel in this region.

3.2.1 Tube Wall Temperature (Tw)

Tw calculations were performed with a computer code describing heat transfer in a Bruce SG for a clean tube (time 't' = 0) and with the distance 'x' from the tube inlet $x \geq 1.567$ m. A power law fitted the results well to give

$$Tw = 284.1(x)^{-0.02866}\ ^{o}C$$

with x in metres.

3.2.2 NiO Solubility Versus Temperature (T)

The calculated curves for NiO solubility versus T at various pH_T were chosen with $pH_T = 7.3$. Points were picked off the graph in Fruzzetti and Sawochka (2000) over the range 260 – 330°C and fitted by a power law to give:

$$S_{NiO} = 162.1 \times 10^{-0.02606\,(T)}$$

where S_{NiO} = NiO solubility, µg Ni/kg. At 304°C SG inlet, $S_{NiO} = 5.878 \times 10^{-11}$ g Ni/g $H_2O = N_0$.

3.2.3 Fe_3O_4 Solubility Versus Temperature (T)

The same heat transfer code was used with the Sweeton & Baes (1970) magnetite solubility curve at pH 10.3. There is an almost-linear decline in solubility with distance along the tube (x) so that

$$Sw_{Fe} = S_A - bx$$

where

Sw_{Fe} = dissolved iron saturation concentration µg Fe/kg H_2O at temperature or location
S_A = solubility at T_W value at x = A
x = distance from tube inlet
b = slope
Then

$Sw_{Fe} = 7.3 - 2.7 \times 10^{-4}$ (x) with x in cm.

3.3 Mass Balance Equations for Dissolved Nickel in the Bulk and Boundary Layer Coolants

Figure 6 shows the two coolant regions where mass balances are required for dissolved nickel. After justifying the assumption to eliminate the mass balance for dissolved iron, the mass balances for dissolved nickel will be presented, first for the bulk coolant, and then for the boundary layer.

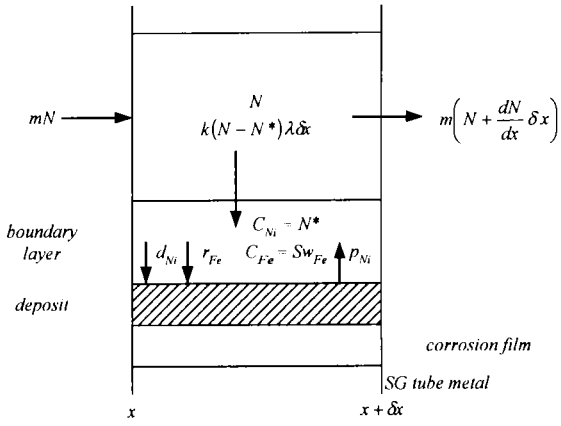

Figure 6. Model of Postulated Behaviour of Dissolved Nickel and Iron on Elemental Volumes of Coolant in the Bulk Flow and in the Boundary Layer.

3.3.1 Dissolved Iron Concentration in Boundary Layer

Magnetite will be growing from the supersaturated coolant in the boundary layer of water next to the deposit. Mass transfer of dissolved iron from the bulk coolant to this layer will be assumed to control the deposition rate, so $C_{Fe} \approx Sw_{Fe}$.

3.3.2 Dissolved Nickel Concentration (Bulk Coolant)

For the bulk coolant:

$$\text{In} - \text{out} = \text{accumulation} = 0$$

$$mN - m\left(\frac{dN}{dx}\delta x + N\right) - k(N - N^*)\lambda\delta x = 0 \qquad (1)$$

$$\therefore \quad -\frac{m}{\lambda}\frac{dN}{dx} = k(N - N^*)$$

where

m = coolant mass flow rate, g/s

λ = specific surface area/length = cm^2/cm

N = Ni concentration in bulk coolant, g Ni/g H_2O

N* = Ni concentration in boundary layer

x = distance from SG tube inlet, cm

k = mass transfer coefficient, g H_2O/cm^2s (assumed same for Fe and Ni)

3.3.3 Dissolved Nickel Concentration (Boundary Layer Coolant)

For the boundary layer:

$$k(N - N^*)\lambda\delta x + p\lambda\delta x = \frac{r}{y}\frac{N^*}{Sw_{Fe}}\lambda\delta x$$

where the deposition rate of Ni, d, has been taken as a fraction of the Fe deposition rate, based on the ratio of their concentration in the boundary layer, N^*/Sw_{Fe}.

The factor 'y' is a measure of how well the Ni might substitute for Fe in the depositing species. While 'y' could be based on a mechanistic understanding of site preferences, two limiting cases might be:

(i) y = 1 for Ni incorporated in $Fe(OH)_2$, implying $Ni(OH)_2$ formation,

(ii) y = 3 for Ni incorporated in $FeO.Fe_2O_3$, implying $NiO.Fe_2O_3$ formation.

Then,

$$kN - kN^* + p = \frac{r}{y}\frac{N^*}{Sw_{Fe}}$$

where

p = release rate of Ni by Inconel 600 corrosion
Sw_{Fe} = dissolved iron solubility at tube wall temperature Tw.

Solving for N* gives

$$N^* = y\,Sw_{Fe}\frac{(p + kN)}{(r + ykSw_{Fe})} \quad (2)$$

Substituting N* into equation (1) yields

$$-\frac{m}{\lambda}\frac{dN}{dx} = kN - \frac{ykSw_{Fe}(p + kN)}{(r + ykSw_{Fe})}$$

3.3.4 Ni/Fe Ratio in Magnetite Deposits in SG

An order-of-magnitude analysis may be used to seek an approximate analytical solution by first simplifying the denominator:

r = $k(C_{Fe} - Sw_{Fe})$
= $0.26\,(7.5 - 7.0) \times 10^{-9} = 1.3 \times 10^{-10}$ g Fe/cm^{2}s for a Bruce SG, based on a comparison of the predicted and observed iron oxide deposition profiles.

$y\,k\,Sw_{Fe}$ = $(1)\,(0.26)\,(7.0 \times 10^{-9}) = 18.2 \times 10^{-10}$ g Fe/cm^{2}s

where y = 1 to make the estimate conservative. Thus,

$$y\,k\,Sw_{Fe} >> r$$

and so

$$-\frac{m}{\lambda}\frac{dN}{dx} \approx kN - \frac{ykSw_{Fe}(p + kN)}{ykSw_{Fe}}$$

$$-\frac{m}{\lambda}\frac{dN}{dx} = kN - p - kN$$

$$\frac{dN}{dx} = \frac{\lambda p}{m}$$

$$N = \frac{\lambda p}{m}x + C_1$$

With the boundary condition

x = A
N = N_A

where A is the distance from the SG tube inlet where precipitation begins, and so

$$N = N_A + \frac{\lambda p}{m}(x - A) \quad (3)$$

Equation (2) for N* may be simplified with $ykSw_{Fe} >> r$ to give

$$N^* \approx \frac{p + kN}{k} = \frac{p}{k} + N$$

and substituting for N gives

$$N^* = N_A + \frac{p}{k} + \frac{\lambda p}{m}(x - A) \quad (4)$$

The ratio Ni/Fe in the magnetite deposits will be the same as the ratio of their deposition rates. Then

$$\frac{Ni}{Fe} = \frac{d}{r} = \frac{\frac{r}{y}\frac{N^*}{Sw_{Fe}}}{r} = \frac{1}{y}\frac{N^*}{Sw_{Fe}}$$

and so

$$\frac{Ni}{Fe} = \frac{N_A}{ySw_{Fe}} + \frac{p}{ykSw_{Fe}} + \frac{\lambda p}{ymSw_{Fe}}(x - A) \quad (5)$$

Assuming that there is no heavy water steam to condense, and assuming $N < Sw_{Ni}$, then a mass balance may be done on the coolant to determine N_A.

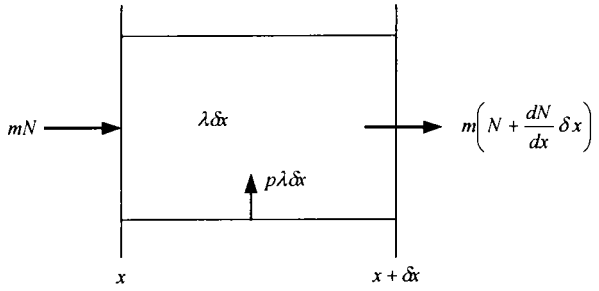

$$\text{in} - \text{out} = \text{accumulation} = 0$$

$$\therefore Nm + p\lambda\delta x = mN + m\frac{dN}{dx}\delta x$$

and so

$$\frac{dN}{dx} = \frac{p\lambda}{m}$$

$$N = \frac{p\lambda x}{m} + C_2$$

The boundary condition to evaluate the integration constant is given as

$N = N_0$
$x = 0$

and the result is

$$N_A = N_0 + \frac{p\lambda A}{m} \quad (6)$$

3.4 Solution of Mass Balance Equations

A Fortran code was written to solve the model equations for a Bruce SG with the parameter values below:

m = 335.7 g H_2O / s / tube
d_i = 1.071 cm
A = location for onset of Fe_3O_4 precipitation ≈ 530 cm (in code with C_{Fe} 7.5 μg/kg, pH 10.3 solubility curve from Sweeton and Baes (1970))
L = 1413 cm
k = "kbar" = average mass transfer coefficient along tube = 0.26 g H_2O/cm^2s

Inconel 600 corrosion product release rates were measured by Taylor (1977) under CANDU reactor HTS conditions with the value for all current SG tube alloys (Monel-400, Inconel-600, Incoloy-800) being given as 0.05 mg/dm^2.day(mdd), almost at the limit of detection when using corrosion coupons.

The release rate fraction of each corroded element is assumed to be the same as its composition in the alloy given in Table 1. Since 1 mdd = 1.16×10^{-10} g/cm^2s, then for Inconel-600:

(Ni) p = $0.76 \times 5.8 \times 10^{-12}$ = 4.41×10^{-12} g Ni/cm^2s, and
(Fe) q = $0.08 \times 5.8 \times 10^{-12}$ = 0.46×10^{-12} g Fe/cm^2s.

Table1. Composition of SG Alloys

Element	SG Alloy, wt% Element		
	Monel-400	Inconel-600	Incoloy-800
Ni	69	76.0	32.5
Fe	1	8.0	46.0
Cr	--	15.5	21.0
Co	1500*	--	--
Cu	30	--	--

* values for Co in mg Co/kg for Pickering-A SG.

4. Comparison of Predicted Ni/Fe Ratios with Measured in SG Deposits

The results of two calculations with the code with (i) y = 1, (ii) y = 3, given in Table 2, show that:

(a) Allowing Ni^{2+} only to occupy Fe^{2+} sites in magnetite "growing from solution" gives Ni/Fe ≈ 0.0055 for y = 3, while allowing them to compete equally for sites (y = 1) gives Ni/Fe ≈ 0.0170 over a wide range of distances (x) along the tubes. The results from four SG tubes examined at Bruce N.G.S. are given in Figure 7. A comparison of prediction with observation suggests that y = 1 gives better agreement than does y = 3.

(b) The calculations for y = 1 show a 43% increase in Ni/Fe ratio along the tube, while the data are variable with no trend apparent.

(c) The data show relatively high Ni/Fe ratios at ≈1 m from tube inlet. Deposits in this region were very light in comparison with those formed further along the hot leg, i.e., x = A = 530 cm. The high ratio may indicate some NiO precipitation as the coolant is injected with dissolved Ni from Inconel 600 corrosion in this region, combined with iron-rich particles that have also deposited in this region.

(d) The solubility of Ni in the boundary layer will be higher than in the bulk coolant. The calculations show its solubility at the wall temperature rising from 0.1375 μg Ni/kg to 0.1676 μg Ni/kg along the length from $530 \leq x \leq 1413$ cm. The concentration of dissolved Ni does not exceed its solubility in the boundary layer water.

(e) The concentration of dissolved nickel (N*) in the boundary layer is independent of the deposition rate of iron, provided the implication $ykSw_{Fe} >> r$ is true. Equation (4) shows that N* depends only on corrosion rate and location along the tube.

Table 2. Results of Two Runs of Fortran Code for Ni/Fe Ratio in SG Deposits

Results of Two Runs of Code with the Limiting Case Values for 'y'							
No = 0.588E-10 Na = 0.822E-10 y = 1.0				No = 0.588E-10 Na = 0.822E-10 y = 3.0			
x(cm)	Ni/Fe	SwNi(ugNi/kg)	CwNi(ugNi/kg)	x(cm)	Ni/Fe	SwNi(ugNi/kg)	CwNi(ugNi/kg)
539.9	0.0139	0.1395	0.0992	530.0	0.0046	0.1395	0.0992
618.3	0.0144	0.1439	0.1031	618.3	0.0048	0.1439	0.1031
706.6	0.0150	0.1478	0.1070	706.6	0.0050	0.1478	0.1070
794.9	0.0156	0.1513	0.1109	794.9	0.0052	0.1513	0.1109
883.2	0.0163	0.1545	0.1148	883.2	0.0054	0.1545	0.1148
971.5	0.0169	0.1575	0.1187	971.5	0.0056	0.1575	0.1187
1059.8	0.0175	0.1602	0.1226	1059.8	0.0058	0.1602	0.1226
1148.1	0.0181	0.1628	0.1265	1148.1	0.0060	0.1628	0.1265
1236.4	0.0187	0.1652	0.1304	1236.4	0.0062	0.1652	0.1304
1324.7	0.0193	0.1675	0.1343	1324.7	0.0064	0.1675	0.1343
1413.0	0.0200	0.1696	0.1382	1413.0	0.0067	0.1696	0.1382

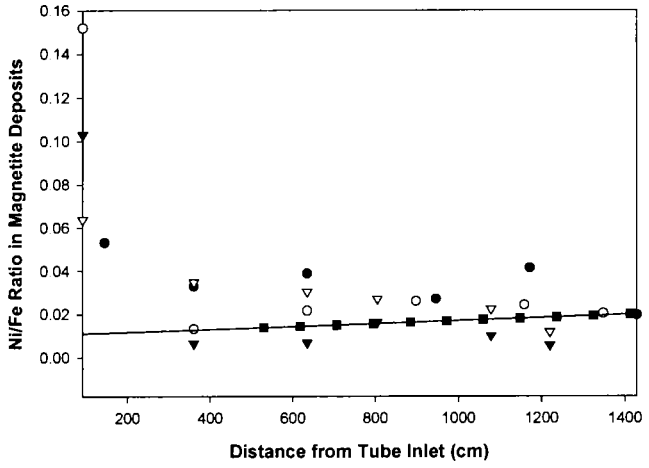

Figure 7. Ni/Fe Ratio in Steam Generator Tube Deposits at Bruce-A, Measured by Oxiprobe. (Straight line is fitted to the predicted points shown. A change in data point symbol indicates a change in tube sampled.)

Similar calculations done for a Darlington NGS steam generator (with internal preheater) are compared with deposit data in Figure 8. The predicted Ni/Fe ratio is lower than measured, possibly because the actual corrosion product release rate is higher than assumed from Taylor's measurements.

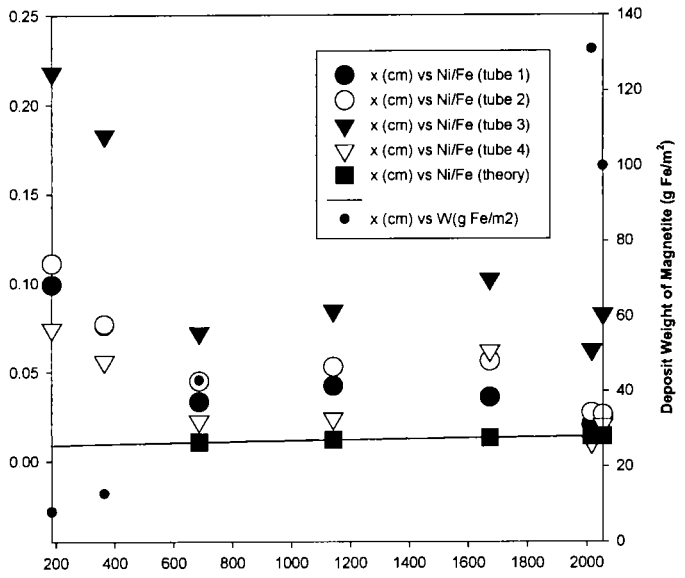

Figure 8. Ni/Fe Ratio in CANDU SG Tube Deposits with Incoloy 800 Tubes and Internal Preheater at x>1700 cm. (Precipitation begins at x>600 cm. Straight line is fitted to the predicted points shown. A change in data point symbol indicates a change in tube sampled.)

5. The Measured Local Variation in Deposit Composition with Depth

Depth profiling of the primary side oxide of a section of CANDU 6 Incoloy-800 steam generator tube from the cold leg was carried out using Secondary Ion Mass Spectrometry (SIMS) and a sequential electrolytic descaling procedure. In the absence of a magnetite standard for the SIMS sputtering, the depth through the oxide was determined from the argon ion sputtering used in SIMS sputtering times using the magnetite film thickness, ~120 μm, determined by descaling. This 120 μm thick layer was assumed to end at the point in the SIMS profile where the Cr signal increases sharply. This interface, referred to as the metal-oxide interface, is more correctly the interface between the outer, deposited magnetite layer and the compact, inner oxide or metal surface; a more detailed examination of the data would be needed to clearly define the locations of the various interfaces. Figure 9 shows the ratios of the nickel signals to Fe-56 (i.e., the deposited magnetite film), which suggests the presence of a Ni-enriched region relative to Fe close to the oxide–metal interface.

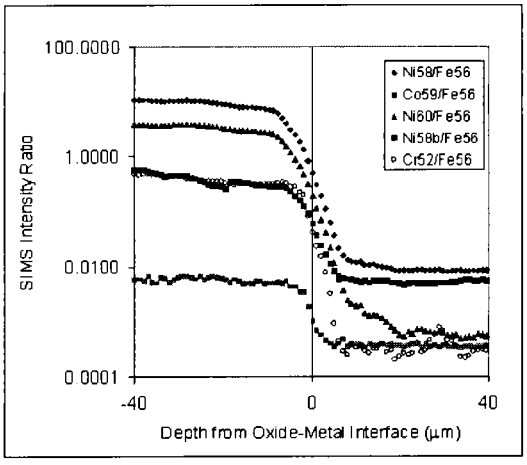

Figure 9. SIMS Depth Profile Through 120 μm Thick Magnetite Deposit on the Cold Leg, Primary Side, of an Incoloy-800 Steam Generator Tube Removed from a CANDU-6 Plant.

6. Conclusions

A simple model has been made to describe the dissolved nickel concentration in the coolant in the SG, for a Bruce plant with no steam quality assumed at the SG inlet. The SG heat transfer models written for a Bruce unit have been used to determine tube wall surface temperature (Tw), nickel oxide solubility at the wall temperature (SwNi), and the concentration of dissolved nickel in both the bulk coolant and the boundary layer of water next to the deposit. Initial calculations showed that a model with both Fe and Ni transferring to the deposit surface from the bulk coolant probably was not accurate. Rather, the boundary layer concentrations of both elements must be determined, since Ni is being supplied to the boundary layer by Inconel 600 corrosion product release, as well as by mass transfer from the bulk coolant. The above model was used with Fe and Ni being treated as equal in the depositing species (y = 1, for ferrous hydroxide, for example) or with the Ni only being able to substitute for one-third of the depositing iron (y = 3, for magnetite). A comparison with deposit data from four SG tubes in a Bruce-A unit show Ni/Fe = 0.02 over the region x > 5 m where there are heavy magnetite deposits. In the inlet region of the hot leg before there is magnetite deposition, then Ni/Fe= 0.05-0.15, richer in nickel than in the much heavier magnetite deposits found further along the tubes. This region could be showing NiO precipitation due to Inconel 600 corrosion product release, combined with crud particle deposits. The model predicts a slow rise in the Ni/Fe ratio in the magnetite deposits along the SG tube, and matches the plant data best when y = 1.

This detailed analysis of dissolved Ni co-precipitation with dissolved iron in CANDU reactor SG tubes supports the hypothesis that precipitating iron keeps the dissolved nickel concentration low enough to avoid in-core precipitation of NiO. If there is insufficient precipitation of dissolved iron as in PWRs, then co-precipitation seems ineffective in preventing in-core precipitation of NiO and the production of relatively large quantities of Co-58.

7. Acknowledgement

The authors appreciate the discussions between colleagues on the IAEA CRP on Activity Transport Modeling in the period 1996-2002. These discussions were the impetus for the current work. Insightful comments and discussion with Billy Fellers, Consulting Chemist for TXU, on the nature of the Axial Offset Anomaly and the in-core chemistry of PWRs is gratefully acknowledged. Finally, permission to use deposit data from various plants is grateful acknowledged, and we thank specifically: W. Little of Bruce Power for the deposit data from Bruce steam generators, M. Dymarski of Ontario Power Generation (OPG) for the deposit data from Darlington steam generators, C. Baker of the CANDU Owner's Group (COG) for the deposit data from a CANDU-6 plant. All these data have allowed much more than a theoretical paper to be written.

8. References

Bergmann, C.W.; Roesmer, J.; Perone, D.W. *Primary Side Deposits on PWR Steam Generator Tubes;* EPRI report NP-2968, 1983.

Burrill, K.A.; Turner, C.W. *Control of Reactor Inlet Header Temperature (RIHT) Rise in CANDU*; AECL report AECL-11131, 1994.

Burrill, K.A. *An Activity Transport Model for CANDU Based on Iron Transport in the Primary Coolant;* AECL report AECL-11805, 1998.

Fero, A.H. *Gamma Ray Exposure-Rate Distribution in a Steam Generator*; EPRI report EPRI-NP-3107, 1983.

Frattini, P.L.; Blok, J.; Chauffriat, S.; Sawicki, J.; Riddle, J. *Axial Offset Anomaly: Coupling PWR Primary Chemistry with Core Design.* In Proceedings of the 8th International Conference on Water Chemistry of Nuclear Reactor Systems, Bournemouth, UK, 2000 October 22-26, Vol. 1, pp 24-33.

Fruzzetti, K.; Sawochka, S. *Modeling Deposit Formation on PWR Fuel Cladding Surfaces.* In Proceedings of the Axial Offset Anomaly (AOA) Science Workshop, EPRI, Palo Alto, U.S., 2000 February; P. Frattini, Ed.; paper #9.

Sweeton, F.W.; Baes, C.F., Jr. Solubility of Magnetite and Hydrolysis of Ferrous Ion in Aqueous Solutions at Elevated Temperatures. *J. Chem.Thermodyn.* **1970**, *2,* 479-500, 1970.

Taylor, G.F. Corrosion Monitoring in CANDU Nuclear Generating Stations. Presented at NACE CORROSION '77, San Francisco, U.S., 1977 March; paper #119. Issued as AECL report AECL-5648.

Vernon, C.W. *Steam Generator Dose Rates on Westinghouse Pressurized Water Reactors;* EPRI report EPRI-AP-2453, 1982.